

## SOL-GEL AUTO-COMBUSTION SYNTHESIS OF COBALT FERRITE AND IT'S CYTOTOXICITY PROPERTIES

S. KANAGESAN<sup>a\*</sup>, M. HASHIM<sup>a</sup>, S. TAMILSELVAN<sup>b</sup>, N.B. ALITHEEN<sup>b</sup>,  
I. ISMAIL<sup>a</sup>, M.SYAZWAN<sup>a</sup>, M.M.M. ZUIKIMI<sup>a</sup>

<sup>a</sup>*Materials Synthesis and Characterization Laboratory (MSCL), Institute of Advanced Technology (ITMA), Universiti Putra Malaysia, 43400 Serdang, Selangor, Malaysia*

<sup>b</sup>*Department of Cell and Molecular Biology, Faculty of Biotechnology and Biomolecular Sciences, University Putra Malaysia, 43400 Serdang, Selangor, Malaysia*

Cobalt ferrite (CoFe<sub>2</sub>O<sub>4</sub>) nanoparticles were successfully synthesized by a sol-gel combustion technique. The particle size as determined by a transmission electron microscope was about 25 nm. A maximum saturation magnetization of 22.31 emu/g and a coercivity of 118 Oe were achieved for the samples. The effect of CoFe<sub>2</sub>O<sub>4</sub> nanoparticles on 4T1 murine breast cancer cells was explored by cytotoxicity assay and flow cytometer analysis. The lower concentrations of CoFe<sub>2</sub>O<sub>4</sub> nanoparticles did not induce any toxicity in cells, when exposed for 24 h. Concentrations exceeding 400 µg/ml produced significant morphological changes and induced cell death by apoptosis and necrosis.

(Received August 23, 2013; Accepted November 9, 2013)

*Keywords:* cobalt, phase formation, sol-gel, magnetization,

### 1. Introduction

The oxides known as spinel ferrites with a cubic unit cell, otherwise referred to as ferros spinels and have a formula of M<sub>x</sub>Fe<sub>3-x</sub>O<sub>4</sub>, derived their name from the naturally occurring mineral MgAl<sub>2</sub>O<sub>4</sub> with a face centered cubic structure and are generally represented as MFe<sub>2</sub>O<sub>4</sub> [1]. Here M can be either Fe, Mn, Co, Ni, Cu or Zn. The identification of new materials with enhanced properties or new synthesis techniques to improve the performance of existing materials, along with the cost-effective advantages, is always an interesting matter for researchers [2]. Spinel ferrite nanoparticles have a wide range of technological applications including magnetic refrigeration, Ferro fluids, high density recording, spintronics, etc. [3, 4, 5]. Properties of spinel ferrite can be controlled by chemical composition, substitution, method of synthesis and the particle size. Therefore serious studies have been carried out to improve the magnetic and electrical properties of ferrite nanoparticles. CoFe<sub>2</sub>O<sub>4</sub> exhibits high coercive force, mechanical hardness, and chemical stability. Therefore more efforts have been made for the synthesis and characterization of CoFe<sub>2</sub>O<sub>4</sub> materials. Several researchers have reported on various methods of synthesis of cobalt ferrite such as hydrothermal synthesis [6, 7], coprecipitation [8, 9], sol-gel [10, 11], spray drying [12], solid-state, microemulsion processes [13, 14], mechanical alloying [15, 16] and electrochemical synthesis [17]. The wet chemical methods requires low processing temperature. For example, CoFe<sub>2</sub>O<sub>4</sub> nanoparticles can be synthesized in the temperature range of 164–192°C by a microwave assisted hydrothermal process, however the solid-state method necessarily requires a high temperature of about 800°C [18].

\*Corresponding author: kanagu1980@gmail.com

In the past few years, biological and biomedical applications in health care have rapidly developed, and nanoparticle-based materials have attracted much attention because of their potential for use as efficient drug delivery carriers for diagnostic and therapeutic applications. Cancer is a malignant neoplasm characterized by uncontrolled growth of abnormal cells in the body. Cancer can develop in almost any organ or tissue of the body, however, the efficient cure of cancer is still a challenge in disease treatments. Advances in cancer nanotechnology increase the use of novel therapeutic strategies such as nanotheranostics, which utilize individualized diagnostic therapy [19]. Cobalt ferrite nanoparticles possess a potential for possible future biomedical applications [20, 21] spanning from cell separation, purification and contrast agents for magnetic resonance imaging [22] to drug delivery [23], biosensors [24], and magnetic fluid hyperthermia [25, 26]. The  $\text{CoFe}_2\text{O}_4$  nanoparticles have received particular attention because of their slower magnetic moment relaxation compared to magnetite ones. The present study is focused on the concentration-dependent distribution of  $\text{CoFe}_2\text{O}_4$  nanoparticles in murine breast cancer cells 4T1. The 4T1 is selected because it is one of the cell models considered for *in vitro* tests of metal compounds and it has been used for the evaluation of the cytotoxicity of nanoparticles [27, 28]. Cancer cells appear to take up magnetic nanoparticles by endocytosis, a process which occurs more in highly-proliferating cells. Direct intra-cancer injection of biocompatible  $\text{CoFe}_2\text{O}_4$  used as magnetic drug carriers in canine breast cancers has shown that endocytosis of  $\text{CoFe}_2\text{O}_4$  nanoparticles occurs just one hour after administration [29]. Previous studies have demonstrated that  $\text{CoFe}_2\text{O}_4$  nanoparticles are safe at lower concentrations and induce cytotoxicity at high concentrations [29, 30]. More recently, the *in vitro* and *in vivo* toxicity of  $\text{CoFe}_2\text{O}_4$  was evaluated using the L929 cell line together with the cytotoxicity assay and intravenous (IV) injections in male ICR (Imprinting Control Region) mice. *In vitro* cytotoxicity was observed at high doses while no adverse effects were found *in vivo* on mice, either as changes in growth or behavior when comparing the test and control groups [30]. The main goal of this paper is to synthesize and to study the properties of  $\text{CoFe}_2\text{O}_4$ . Since there are only few reports available on anticancer effects of  $\text{CoFe}_2\text{O}_4$  nanoparticles, here we report the sol-gel synthesis, structural, morphological, magnetic and anticancer behavior of cobalt spinel ferrite nanoparticles.

## 2. Materials and Methods

### 2.1. Materials

All the chemicals are of analytical grade and are used as received without further purification. Cobalt nitrate [ $\text{Co}(\text{NO}_3)_2 \cdot 6\text{H}_2\text{O}$ ], ferric nitrate [ $\text{Fe}(\text{NO}_3)_3 \cdot 9\text{H}_2\text{O}$ ], ethylene glycol [ $\text{C}_2\text{H}_6\text{O}_2$ ], citric acid [ $\text{C}_6\text{H}_8\text{O}_7$ ] are bought from Sigma-Aldrich chemical reagent Co., (USA).

### 2.2. Synthesis of $\text{CoFe}_2\text{O}_4$ nanoparticles

The  $\text{CoFe}_2\text{O}_4$  nano powder was synthesized by the sol-gel auto-combustion method. A proper amount of metal nitrates and citric acid was first dissolved in a minimum amount of ethylene glycol. The molar ratio of cobalt and ferric nitrates was 1:2 and nitrates to citric acid ratio was 1:1. The mixed solution was stirred magnetically for 3 h at room temperature and then additional water was removed in a vacuum rotary evaporator at 60–80°C till a gel was obtained. Then the gel was dried in a hot air oven at 150°C for 24 hours to get the brown colour cobalt ferrite powder.

### 2.3. Characterization

An X-ray diffraction pattern was taken for the calcined sample by X-ray diffractometer (Phillips Expert ProPW3040) using  $\text{CuK}\alpha$  radiation in a wide range of  $2\theta$  ( $10 < 2\theta < 80$ ). The particle morphology observation of the specimen was performed using transmission electron microscope (TEM). The magnetic characteristics of the specimen was measured at room temperature using a vibrating sample magnetometer (VSM model-LDJ9600).

## 2.4. Maintenance of cell cultures

4T1 murine breast cancer cells were procured from the American type culture collection. The cell lines were maintained and propagated in 90% RPMI medium containing 10% fetal bovine serum (FBS) and 1% penicillin/streptomycin. Cells were cultured as adherent monolayers (i.e., cultured at approximately 80% confluence) and maintained at 37°C in a humidified atmosphere of 5% CO<sub>2</sub>. Cells were harvested after brief trypsinization.

## 2.5. Cell viability assay

The 4T1 cells were harvested, counted and transferred to 96-well plates and incubated for 24 h prior to the addition of the nanoparticle. The CoFe<sub>2</sub>O<sub>4</sub> nanoparticles were processed and applied in various concentrations, and the treated cells were incubated for 24 h. Five milligram of MTT (3-[4,5-dimethylthiazol-2-yl]- 2,5-diphenyltetrazolium bromide) was dissolved in 1 mL of phosphate-buffered saline (PBS), and 25µL of the MTT solution was added to each of the 96 wells. The plates were wrapped in aluminum foil and incubated at 37 °C for 4 h. The solution in each well, containing media, unbound MTT and dead cells, was removed by suction, and 200µL of dimethylsulfoxide was added to each well. The plates were then shaken, and the optical density was measured using a micro plate reader at 575 nm. Three independent experiments were performed for each study and all measurements were performed in triplicate. Results were expressed as the percentage proliferation with respect to vehicle-treated cells.

## 2.6. Trypan blue exclusion test

Cell viability was determined by trypan blue exclusion test after cells were harvested with designated treatments in different concentrations of CoFe<sub>2</sub>O<sub>4</sub>. Equal amounts of cell suspension and 0.4% trypan blue were mixed for 1-2 min. 10 µL of the mixture was taken to the hemocytometer and the cells were counted in all the four fields under a light microscope.

## 2.7. Quantification of apoptosis

Cobalt ferrite induced cell death in 4T1 cells was quantified using propidium iodide (PI) and acridine-orange (AO) double staining according to standard procedures and examined under fluorescence microscope (Bio-Rad). Briefly, treatment was carried out in a 25 mL culture flask. 4T1 cells were plated at a concentration of 1x10<sup>6</sup> cell/mL, and treated with CoFe<sub>2</sub>O<sub>4</sub> at various concentrations. Flasks were incubated in atmosphere of 5% CO<sub>2</sub> at 37 °C for 24 h. The cells were then spun down at 1000 rpm for 10 minutes. Supernatant was discarded and the cells were washed twice using PBS after centrifuging at 1000 rpm for 10 minutes to remove the remaining media. 10 µL of fluorescent dyes containing AO (10 µg/mL) and PI (10 µg/mL) were added into the cellular pellet at equal volumes of each. Freshly stained cell suspension was dropped into a glass slide and covered by a coverslip. Slides were observed under UV-fluorescence microscope within 30 minutes before the fluorescence color started to fade. All the treatments and time points were carried out in three individual experiments. AO and PI are intercalating nucleic acid specific fluorochromes which emit green and orange fluorescences, respectively, when they are bound to DNA. Of the two, only AO can cross the plasma membrane of viable and early apoptotic cells. Viewed by fluorescence microscopy, viable cells appeared to have green nucleus with intact structure while apoptotic cells exhibited a bright-green nucleus showing condensation of chromatin as dense green areas. Late apoptotic cells and necrotic cells will stain with both AO and PI. Comparatively, PI produced the highest intensity emission. Hence, late apoptotic cells exhibited an orange nucleus showing condensation of chromatin whilst necrotic cells displayed an orange nucleus with intact structure.

## 2.8. Annexin V-PI staining

The induction of apoptosis in 4T1 cells by cobalt ferrite was examined by FITC-labeled annexin V (FITC-annexin V) staining of the treated cells. The cells were simultaneously stained with PI in order to differentiate the necrotic cells from the apoptotic ones based on the membrane integrity. Following the  $\text{CoFe}_2\text{O}_4$  treatment, cells were harvested and washed with PBS. The cells were then stained with FITC-annexin V-PI as per manufacturer's instructions (FITC Annexin V Apoptosis Detection Kit, BD Pharmingen, NJ) and analyzed in a FACS Calibur (BD Biosciences, NJ) flow cytometer. The data were collected with Cell Quest Pro software for 10000 cells in each sample.

## 3. Results and Discussion

### 3.1 TG analysis

Thermo gravimetric analysis (TGA) curve of  $\text{CoFe}_2\text{O}_4$  sample is shown in Fig.1. The thermal decomposition process of the nitrate–citrate gel process consists of the following three stages. The initial weight loss at the temperature range of 50–150 °C was due to the evaporation of absorbed water and primary breakdown of the complex. The interactions of citrate and nitrate ions in the gel produce spontaneous combustion with the liberation of  $\text{CO}_2$ ,  $\text{H}_2\text{O}$  and nitrate ions which provided the combustion of organic components in the oxidizing environment [31]. The weight loss observed between 190–230 °C with a mass loss of 12.6%, was due to dehydration of the OH group in the spinel structure and formation of semi-organic carbon materials/metal oxides [32, 33]. The final stage in weight loss at the temperature range of 400–640 °C is due to the formation of spinel phase metal oxide. In the TG curve no weight loss was observed above 842 °C. This shows the formation of pure cobalt ferrite.

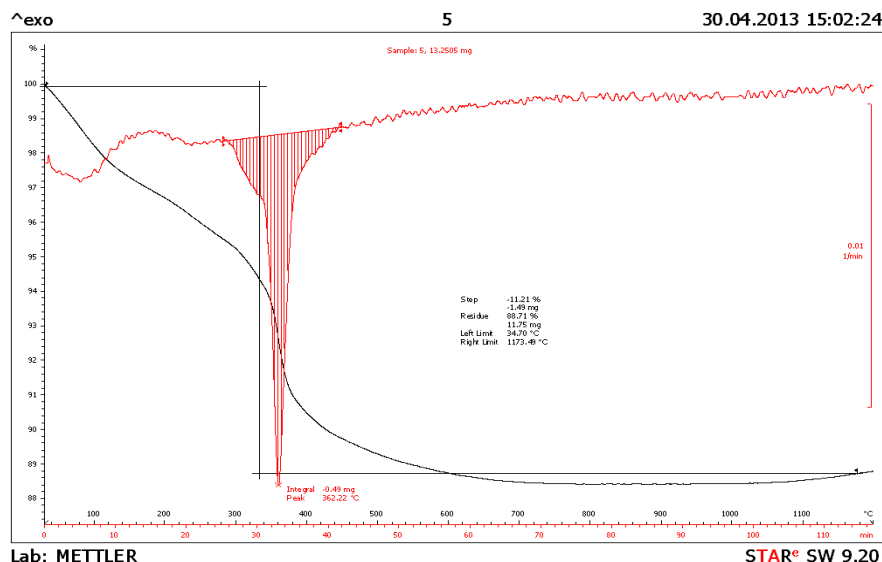


Fig. 1. Thermo gravimetric analysis (TGA) curve of cobalt ferrite sample.

### 3.2 X-Ray diffraction measurements

Fig. 2 shows the X-ray diffraction pattern of the calcinated cobalt ferrite powder. This pattern matches well with the standard diffraction data of  $\text{CoFe}_2\text{O}_4$  crystals. It is clear that a spinel structure of cobalt ferrite labeled in the JCPDS file no#22-1086 was detected in this sample whose space group is  $Fd\bar{3}m$  (227) along with the lattice parameter of  $a = 9.38 \text{ \AA}$ . The crystalline diffraction pattern shows the major  $2\theta$  angles are at  $30.22^\circ$ ,  $35.51^\circ$ ,  $43.20^\circ$ ,  $57.04^\circ$ , and  $62.84^\circ$

which correspond to the diffraction planes of (220), (311), (222), (400), (422), (511) and (440) respectively. Very broad reflections indicate the nanoparticle nature of the samples. The experimental reflections do not show peaks corresponding to any other material or impure phases,

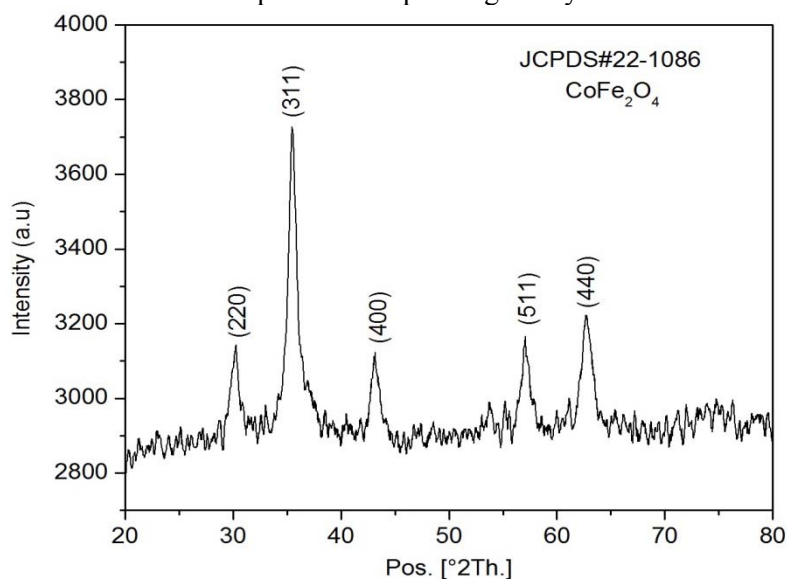


Fig. 2. XRD pattern of cobalt ferrite

### 3.3 Microstructure

Fig. 3 shows the particle size distribution in a TEM micrograph image of CoFe<sub>2</sub>O<sub>4</sub> powder calcined at 150 °C. The particles are nearly spherical in shape and the major portions of the calcined particles are in the size range of 20–40 nm. The histogram inserted in figure 3 shows the size distribution of nano particles. The average size of cobalt ferrite particles draws closer to 30 nm.

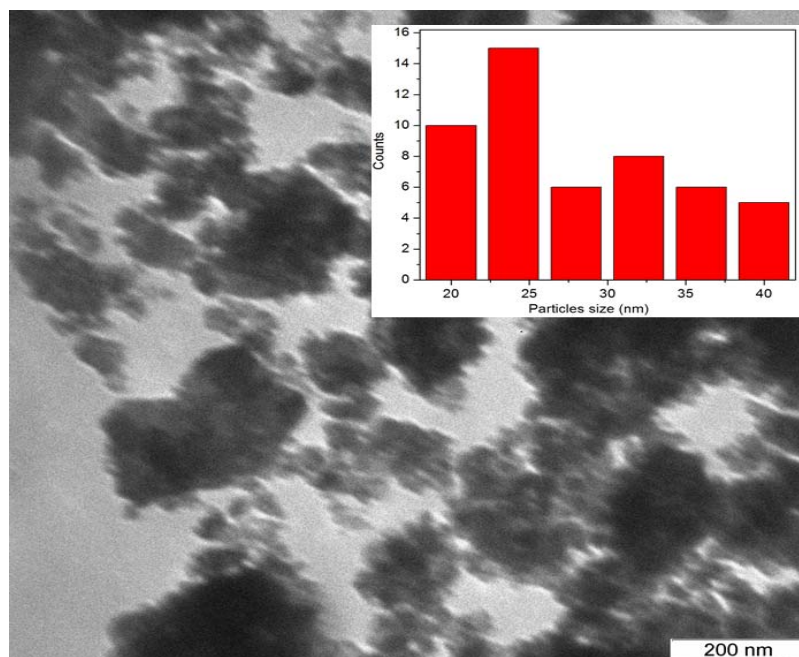


Fig. 3. TEM micrograph of sample calcined at 150°C.

### 3.4 Vibrating sample magnetometer

Normally the magnetization in spinel ferrites arises due the difference in the magnetic moments of cations which are distributed in the octahedral and tetrahedral interstitial sites. This directly points to the distribution of the magnetic  $\text{Fe}^{3+}$  and  $\text{Mn}^{2+}$  ions in the two sublattices along with other factors [34]. Typical hysteresis behavior of the nanosized  $\text{CoFe}_2\text{O}_4$  is shown in Fig. 4. Ferromagnetic behavior is observed for the sample at room temperature. The nanosized  $\text{CoFe}_2\text{O}_4$  magnetization displays a hysteresis loop as the applied field changes in strength and direction. The values of saturation magnetization and coercivity obtained from VSM measurements is found to be  $22.31 \text{ Am}^2/\text{kg}$  and 118 Gauss at 300 K, respectively.

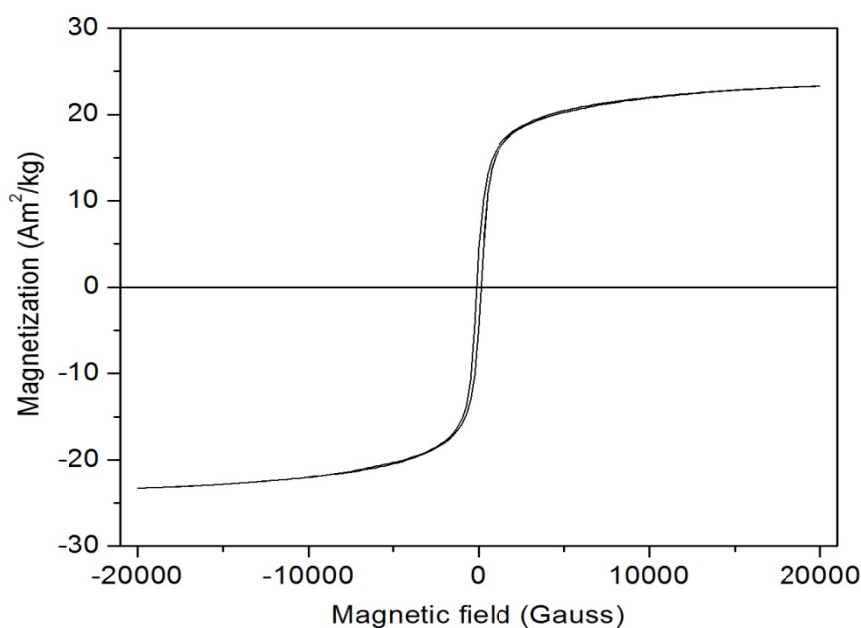


Fig. 4. Hysteresis curve of the cobalt ferrite sample at room temperature (300 K).

### 3.5. Cytotoxicity and alteration in cell morphology

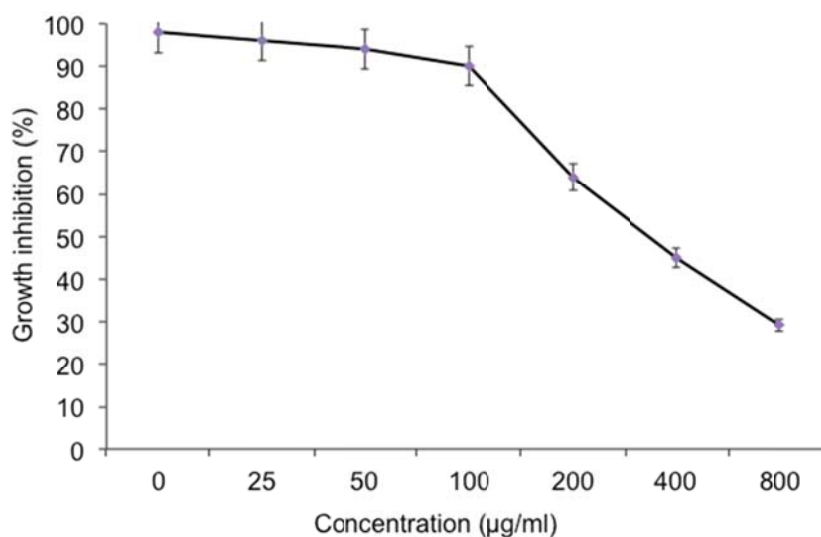
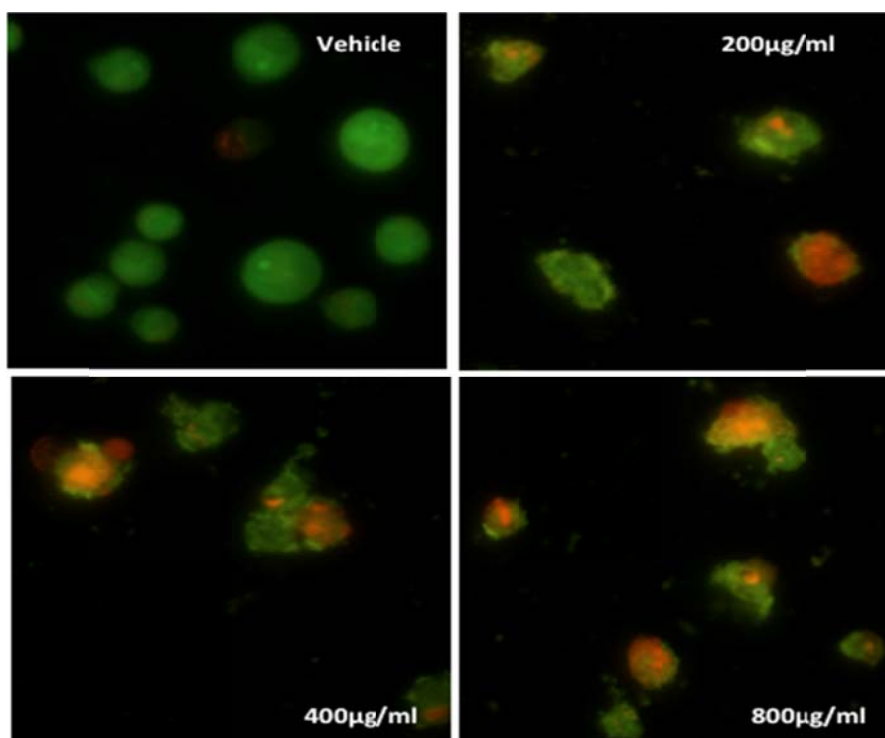


Fig. 5. Effect of cobalt ferrite on growth of breast cancer cell lines 4T1. Cells were seeded in 96-well plates and incubated with different concentrations of cobalt ferrite as noted for 24 h at 37°C. Cell viabilities were determined by 3-(4, 5-dimethylthiazol)-2, 5-diphenyl tetrazolium bromide assay. Data points are presented as means  $\pm$  SD of triplicate

*experiments.*

The 4T1 cells were exposed to cobalt ferrite nanoparticles at the concentrations of 25, 50, 100, 200, 400 and 800  $\mu\text{g/mL}$  for 24 h and cytotoxicity was determined using MTT assays. In this method of analysis, the cell viability was significantly reduced to 96%, 94%, 90%, 63%, 45% and 29% for the cobalt ferrite concentrations of 25, 50, 100, 200, 400 and 800  $\mu\text{g/mL}$  respectively (Fig. 5). This is supported by the previous experimental result in which the  $\text{CoFe}_2\text{O}_4$  nanoparticles showed toxicity only at higher concentrations [29, 30]. In another study, the genotoxic potential of three different sizes of  $\text{CoFe}_2\text{O}_4$  (5.6 nm, 10  $\mu\text{m}$  and 120  $\mu\text{m}$ ) were assessed on human peripheral lymphocytes by Colognato et al [35]. They found that the smaller nanoparticles were associated with significant toxicity and mutagenicity, whilst no effects were induced by the larger nanoparticles. The 4T1 cells treated with various concentrations of the cobalt nanoparticles were examined by fluorescence microscopy after AO/PI staining and characterized to study the structural and morphological changes of cobalt ferrite-induced apoptosis. In general, morphological changes such as cell shrinkage, condensation and fragmented chromatin are associated with apoptotic cell death [36]. Fig. 6 shows the AO/PI staining results obtained using fluorescence microscopy. As seen in Fig. 6, control cells do not show any apoptotic bodies. The cells treated with increasing concentrations of  $\text{CoFe}_2\text{O}_4$  nanoparticles show a progressive accumulation of the apoptotic bodies in a dose dependent manner.



*Fig. 6. Morphological assessment of 4T1 cells stained with acridine orange (green) and propidium iodine (red). Cells were incubated without or with cobalt ferrite at various concentration for 24 hrs. Cells with intact membrane and stained green indicate viable cells; cells that showed chromatin condensation, nuclear genome fragmentation and membrane blebbing indicated early apoptosis; cells that are stained orange and contained fragmented DNA represented secondary necrotic or late apoptotic cells.*

### 3.6. Cell viability and apoptosis

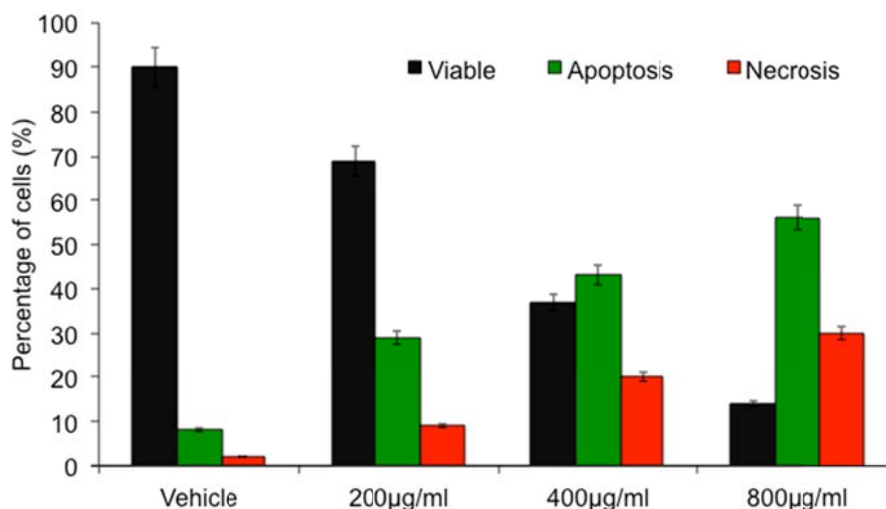


Fig. 7. Flow cytometry analysis of 4T1 cells untreated and treated with cobalt ferrite for 24 hrs stained with Annexin V-FITC/propidium iodide. Data points are presented as means  $\pm$  SD of triplicate experiments ( $p < 0.05$ ).

The apoptotic cell death in 4T1 cells induced by cobalt ferrite nanoparticle was confirmed and subsequently quantified by flow cytometric analysis. Early apoptotic cells can easily be identified by green fluorescence of FITC- conjugated annexin V as annexin V<sup>+</sup> has a high affinity toward phosphatidyl serine residues which are externalized from inner to outer leaflet of the plasma membrane during early stages of apoptosis [37, 38]. Fig. 7 shows the results of flow cytometric analysis of FITC-annexin V-PI stained 4T1 cells treated with different concentrations of CoFe<sub>2</sub>O<sub>4</sub> nanoparticles. The percentages of apoptotic and necrotic population in treated and untreated cells were calculated from the flow cytometric data and the results clearly show the dose-dependent reduction in cell viability of 4T1 cells in the presence of CoFe<sub>2</sub>O<sub>4</sub> nanoparticles. Most importantly, the apoptotic and necrotic population in 4T1 cells increased by 29%, 63% and 86% in the presence of 200, 400 and 800 µg mL<sup>-1</sup> cobalt ferrite nanoparticles, respectively. The results of flow cytometric analysis clearly establish the efficient induction of apoptotic and necrotic cell death in 4T1 cells by CoFe<sub>2</sub>O<sub>4</sub> nanoparticles (Fig. 7). While necrosis is a form of cell death resulting from direct cell damage, apoptosis is a form of cell programmed cell death where one or more cells effectively commit suicide [39]. Based on the results of this study, it is reasonable to suggest that the ions released from nanoparticles, once they have entered the cell, contribute to cytotoxicity according to the Trojan-horse theory proposed for metal nanoparticles by Park et al. [40]. Currently, only a little information is available on the *in vitro* and *in vivo* biocompatibility of CoFe<sub>2</sub>O<sub>4</sub> nanoparticles. Our study demonstrates the simultaneous visualization of viable, necrotic and apoptotic cells suggesting that CoFe<sub>2</sub>O<sub>4</sub> nanoparticles induce apoptosis and necrosis in dose dependent manner. The other possible explanation for the significant cytotoxicological, morphological and phenotypic effects of cobalt ferrite internalization may be due to drastic impede transcriptional regulation and protein synthesis resulting in loss of cell phenotype and possibly cell death. In order to evaluate these possibilities, further studies in physiochemical basis of the observed CoFe<sub>2</sub>O<sub>4</sub> cytotoxicity are necessary.

### 4. Conclusion

In summary, CoFe<sub>2</sub>O<sub>4</sub> nano powder with an inverse spinel structure was synthesized by sol-gel method. The synthesized nanoparticles are about 25 nm in size and they show a typical magnetic hysteresis behavior – ferro magnetic behavior at room temperature. Thermo gravimetric analysis shows that the spinel ferrite phase formation can take place at a relatively low

temperature. It has been found that the 4T1 cells are able to maintain their viability while exposed to  $\text{CoFe}_2\text{O}_4$  nanoparticles at lower concentrations. The apoptosis and necrosis induced at higher nanoparticle concentrations of cobalt ferrite indicate the possible cell death process. These biocompatible cobalt ferrite nanoparticles promise to be potential candidates in combined cancer therapy.

## References

- [1] Richard Perez Moyet, Yenny Cardona, Pedro Vargas, Josue Silva, Oswald N.C. Uwakweh, , Materials Characterization, doi: 10.1016/j.matchar.2010.04.013
- [2] S.D. Bhame, P.A. Joy, Sensors and Actuators A **137**, 256 (2007).
- [3] A. T. Raghavender, R. G. Kulkarni, K. M. Jadhav, , Chinese journal of physics, **48** (4) 2010.
- [4] P. C. Rajesh Varma et al., J. Alloys. Comp. **453**, 29 (2008).
- [5] M. L. Kahn, Z. Jhon Zhang, Appl. Phys. Lett. **78**, 3651 (2001).
- [6] G.B. Ji, S.L. Tang, S.K. Ren, F.M. Zhang, B.X. Gu, Y.W. Du, Journal of Crystal Growth **270**, 156 (2004)–161.
- [7] T. Pannaparayil, R. Marande, S. Komarneni, J. Appl. Phys. **69**, 5349 (1991).
- [8] M. Kiyama, Bull. Chem. Soc. Jpn. **51**, 134 (1978).
- [9] T. Sato, IEEE Transactions on Magnetics **6**, 795 (1970).
- [10] T. Meron, Y. Rosenberg, Y. Lereah, G. Markovich, Journal of Magnetism and Magnetic Materials **292**, 11 (2005).
- [11] S.G. Christoskova, M. Stoyanova, M. Georgieva, Appl. Catal. A **208**, 235 (2001).
- [12] H.F. Yu, A.M. Gadalla, J. Mater. Res. **11**, 663 (1996).
- [13] V. Pillai, D.O. Shah, Journal of Magnetism and Magnetic Materials **163**, 243 (1996).
- [14] N. Moumen, P. Veillet, M.P. Pileni, J. Magn. Magn. Mater. **149**, 67 (1995).
- [15] J. Ding, P.G. McCormick, R. Street, Solid State Commun. **95**, 31 (1995).
- [16] J. Ding, T. Reynolds, W.F. Miao, P.G. McCormick, R. Street, Appl. Phys. Lett. **65**, 3135 (1994).
- [17] S.D. Sartale, C.D. Lokhande, Ceramic International **28**, 467 (2002).
- [18] S. Komarneni, M.C. D'Arrigo, C. Leonelli, G.C. Pellacani, H. Katsuki, J. Am. Ceram. Soc. **81**, 3041 (1998).
- [19] Lv G, He F, Wang X, et al. Langmuir. **24**(5), 2151 (2008)
- [20] Baldi, G., Bonacchi, D., Innocenti, C., Lorenzi, G., Sangregorio, C., , J. Magn. Magn. Mater. **311**, 10 (2007).
- [21] Mornet, S., Vasseurs, S., Grasset, F., Veverka, P., Goglio, G., Demourgues, A., Portier, J., Pollert, E., Douguet, E., Prog. Solid State Chem. **34**(2), 237 (2006).
- [22] Joshi, H.M., Lin Yen, P., Aslam, M., Prasad, P.V., Schultz-Sikma, E.A., Edelman, R., Meade, T., Dravid, V.P., J. Phys. Chem. C **113**, 17761 (2009).
- [23] Arruebo, M., Fernández-Pacheco, R., Ibarra, M.R., Santamaría, J., Nanotoday **2**, 22 (2007).
- [24] Chemla, Y.R., Grossman, H.L., Poon, Y., McDermott, R., Stevensi, R., Alper, M.D., Clarke, J., Proc. Natl. Acad. Sci. U.S.A. **97**, 14268 (2000).
- [25] Hergt, R., Dutz, S., Muller, R., Zeisberger, M., J. Phys.: Condens. Matter **18**, S2919 (2006).
- [26] Salloum, M., Ma, R.H., Weeks, D., Zhu, L., Int. J. Hyperthermia **24**(4), 337 (2008).
- [27] Hartung, T., Bremer, S., Casati, S., Coecke, S., Corvi, R., Fortaner, S., Gribaldo, L., Hadler, M., Roi, A.J., Prieto, P., Sabbioni, E., Worth, A., Zuang, V., Altern. Lab. Anim. **31**, 473 (2003).
- [28] Mazzotti, F., Sabbioni, E., Ghiani, M., Cocco, B., Ceccatelli, R., Fortaner, S., Altern. Lab. Anim. **29**, 601 (2001).
- [29] Vaishnav P . P . et al., , Journal of applied Physics **99**, 08G702 (2006).
- [30] Kim JS, Yoon TJ, Yu KN, et al. Toxicol Sci.; **89**, 338 (2006).
- [31] L. Guo, X. Shen, X. Meng, Y. Feng, J. Alloys Compd. **490**, 301 (2010).
- [32] M. Sivakumar, S. Kanagesan, R. Suresh Babu, S. Jesurani, R. Velmurugan, C. Thirupathi, T. Kalaivani, J Mater Sci: Mater Electron **23**, 1045 (2012)
- [33] P. Sivakumar, R. Ramesh, A. Ramanand, S. Ponnusamy, C. Muthamizhchelvan, Materials

- Research Bulletin **46**, 2204 (2011).
- [34] Richard Perez Moyet, Yenny Cardona, Pedro Vargas, Josue Silva, Oswald N.C. Uwakweh, Materials Characterization, doi: 10.1016/j.matchar.2010.04.01.
- [35] Colognato R. et al., , Mutagenesis, **23**, 377 (2008).
- [36] T.-T. Mai, J.-Y. Moon, Y.-W. Song, P.-Q. Viet, P.-V. Phuc, J.-M. Lee, T.-H. Yi, M. Cho S.-K. Cho, Cancer Lett.,**321**, 144 (2012).
- [37] Martin,S.J.;Reutelingsperger,C.P.M.;McGahon,A.J.;Radar, A.; van-Schie, R. C.; LaFace, D. M.; Green, D. R. J. Exp. Med. **182**, 1545 (1995).
- [38] Koopman,G.;Reutelingsperger,C.P.;Kuijten,G.A.;Keehnen, R. M.; Pals, S. T.; van Oers, M. H. Blood, **84**, 532 (1994).
- [39] Ueda N, Shah SV. Apoptosis. J Lab Clin Med; **124**(2), 169 (1994)
- [40] Park E. J. et al., , Toxicology in Vitro, **24**, 872 (2010a).